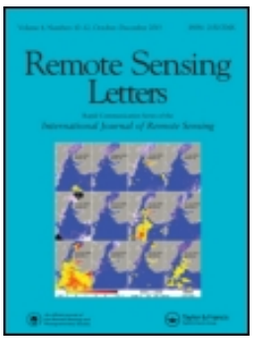

Remote Sensing Letters

ISSN: 2150-704X (Print) 2150-7058 (Online) Journal homepage: http://www.tandfonline.com/loi/trsl20

Automated extraction of manhole covers using mobile LiDAR data

Haiyan Guan, Yongtao Yu, Jonathan Li, Pengfei Liu, Haohao Zhao & Cheng Wang

To cite this article: Haiyan Guan, Yongtao Yu, Jonathan Li, Pengfei Liu, Haohao Zhao & Cheng Wang (2014) Automated extraction of manhole covers using mobile LiDAR data, Remote Sensing Letters, 5:12, 1042-1050, DOI: 10.1080/2150704X.2014.994716

To link to this article: http://dx.doi.org/10.1080/2150704X.2014.994716

Remote Sensing Letters, 2014
Vol. 5, No. 12, 1042–1050, http://dx.doi.org/10.1080/2150704X.2014.994716

Taylor & Francis
Taylor & Francis Group

Automated extraction of manhole covers using mobile LiDAR data

Haiyan Guan[a], Yongtao Yu[b]*, Jonathan Li[b], Pengfei Liu[c], Haohao Zhao[a], and Cheng Wang[b]

[a]*College of Geography and Remote Sensing, Nanjing University of Information Science & Technology, Nanjing, China;* [b]*School of Information Science and Engineering, Xiamen University, Xiamen, China;* [c]*College of Urban & Environment Science, Tianjin Normal University, Tianjin, China*

(*Received 2 September 2014; accepted 25 November 2014*)

Our work addresses the problem of accurately extracting manhole covers, one specific type of road fixture, from a large volume of mobile light detection and ranging (LiDAR) data. We propose an efficient, step-wise manhole cover extraction method. First, road surface points are extracted and interpolated to generate two-dimensional geo-referenced feature (GRF) images. Next, the method segments manhole cover candidates by applying distance-dependent thresholding and multi-scale tensor voting to the GRF images. Finally, distance-based clustering and a morphological operation are used to extract manhole covers. Experiments were carried out to qualitatively and quantitatively demonstrate the performance of our manhole cover extraction method.

1. Introduction

Pavement manholes provide access to conduits that are used to conduct rainwater, waste, steam, natural gas, and other utility networks including telecommunication wires and power cables. It is one of the key elements in urban environment that ensures quality of life, economic prosperity, and national security (Pikus 2006). Pavement manholes are usually covered with metal or concrete covers to prevent things from dropping into the wells and to provide moving vehicles and pedestrians with a safe environment. Missing manhole covers, which cause significant loss of life and injury every year, are particularly dangerous (Ji, Shi, and Shi 2012). It is, therefore, imperative that pavement manholes be monitored routinely.

In the early stages, the inventory mapping of pavement manholes – a labour-intensive, time-consuming, and costly task – was accomplished manually by field specialists in transportation agencies. In recent years, mobile mapping systems, using charge-coupled device cameras or video cameras, have been developed for roadway inventory mapping (Broggi 1995; McCall and Trivedi 2006; Golparvar-Fard, Balali, and de la Garza 2012). Accordingly, image processing methods, including morphological techniques, Hough transform, and edge detection operators, have been developed for detecting and evaluating pavement features (He, Wang, and Zhang 2004; Tanaka and Mouri 2000; Timofte and Gool 2011; Cheng et al. 2007). However, these techniques highly depend on the illumination conditions of the surveyed scenes and are heavily affected by noise such as pavement cracks and shadows cast by passing vehicles, roadside buildings, and trees. Therefore, image- and video-based inventory mapping techniques still face great challenges and

*Corresponding author. Email: allennessy.yu@gmail.com

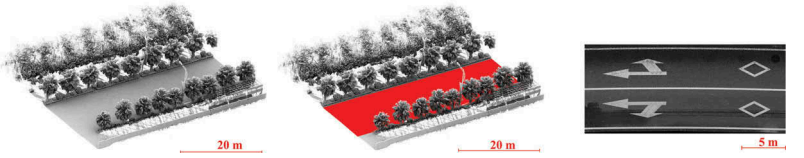

(a) (b) (c)

Figure 1. (*a*) A sample of mobile LiDAR data, (*b*) extracted results of road surfaces (red), and (*c*) a GRF image of the extracted road surface.

require much improvement in order to meet increasing demands for the inspection and inventory of highways and public roads.

Since 2003, mobile light detection and ranging (LiDAR) has been a promising means for land-based surveying and mapping. Mobile LiDAR systems integrated with laser scanner(s), digital camera(s), global positioning system, inertial measurement unit, and distance measurement indicator collect three-dimensional (3-D) geospatial data of roadways over a large area at a normal driving speed (Williams et al. 2013). By using the near-infrared spectrum, such systems work, day and night, without considering the environmental illumination. The United States National Cooperative Highway Research Program presents guidelines for the use of mobile LiDAR in transportation applications (Olsen et al. 2013). Particularly, this program aims to analyse quality control procedures to verify the accuracy of the data collected with mobile LiDAR. The excellent quality and accuracy of mobile LiDAR data allow users to accurately extract manhole covers for rapid update of road inventory.

In this article, we propose a stepwise algorithm for directly extracting manhole covers from mobile LiDAR data. Figure 1 shows the flow chart of our strategy for automatically extracting manhole covers. The strategy includes three steps: (1) data pre-processing including road surface extraction and geo-referenced feature (GRF) image generation; (2) manhole cover segmentation including distance-dependent thresholding segmentation and multi-scale tensor voting; and (3) manhole cover extraction including Euclidean distance clustering and morphological operations.

2. Methodology

2.1. Pre-processing

The mobile LiDAR data acquired by our system contain both road surfaces and roadside features. Inventory mapping of manhole covers focuses only on road surface point clouds. To reduce the amount of data being processed and the time complexity of the proposed strategy, we rapidly and accurately segment road surfaces from the entire point clouds. The extraction of road surfaces is based on two observations: trajectory data and curbs. Trajectory data record a vehicle's precise and real-time positioning information. In an urban environment, curbs function to separate road surfaces from roadsides. Curb height generally ranges from 10 to 20 cm, depending upon a specific country's street design and construction manuals. A vehicle's trajectory and the function of the curbs are used to efficiently separate road surface points from the large volume of mobile LiDAR data. The description of road surface extraction can be found in Guan et al. (2014).

Instead of processing road surface points in 3-D space, we rasterize these points into a two-dimensional (2-D) GRF image based on the intensity information of the laser points.

In Guan et al. (2014), a modified inverse distance weighted interpolation method was proposed to generate GRF images with a given cell size, S_p. The value of each grid cell is based on the following rules: (1) a point with higher intensity obtains a greater weight and (2) a point nearer to the grid centre obtains a greater weight. The generated GRF image reflects well the reflective characteristics of road surfaces and can be used for inventory mapping of manhole covers.

2.2. Segmentation

In the generated GRF image, a threshold-based segmentation is normally carried out to detect manhole covers. However, the intensity values of road surfaces are less consistent as they gradually fade from the scanning centre to the two sides of the road. This variation is due to the reflected intensity values that depend on (1) the scanning range from the laser sensor to the target, (2) the incidence angle of the laser beam, and (3) material properties of the target. We propose a distance-dependent thresholding segmentation method that considers variations of scanning distance. For each range of scanning distances, local optimal segmentation thresholds are adaptively estimated. Centred at the vehicle trajectory, a GRF image is partitioned into a set of segments with a width, W_s, in two opposite directions. Then, all the segments are thresholded separately to identify manhole cover candidates using Otsu's (1979) method, which is widely implemented as the default approach to image thresholding (Xue and Titterington 2011). Figure 2 shows stepwise results for extracting manhole covers on a selected GRF image sample. Figure 2(*b*) shows the manhole cover candidates obtained using the distance-dependent thresholding segmentation method.

As seen in Figure 2(*b*), the identified manhole cover candidates contain considerable noise. The noise is caused by the characteristics of the signal backscattered by the measured targets and the materials of the targets' surface. To efficiently filter out the noise, we develop a multi-scale tensor voting framework, which has the capability of suppressing noise and preserving manhole covers. Tensor voting, which was first introduced in computer vision for perceptual grouping purposes (Mordohai and Medioni 2006), has the capability to efficiently infer geometric structures from noisy data.

In 2-D, perceptual grouping is undertaken through casting votes between image primitives, such as unoriented points, curve elements, and region elements. Since no prior distribution information is available, image primitives are initially encoded with ball tensors with unit saliencies. The saliency of each tensor is propagated within the voting field with a form of vote. By aggregating the votes from the nearby tensors, each tensor becomes a general second-order, symmetric, non-negative definite tensor, which simultaneously encodes multiple perceptual structures (Mordohai and Medioni 2006; Zou et al. 2012). Through tensor decomposition and eigenvalue analysis, different geometric

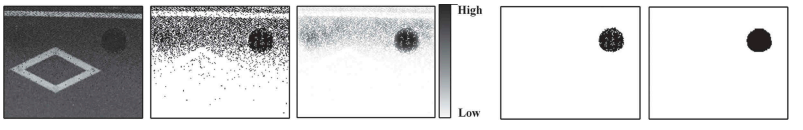

Figure 2. (*a*) Geo-referenced intensity image with a manhole cover, (*b*) identified manhole cover candidates, (*c*) saliency map, (*d*) extracted manhole cover, and (*e*) refined manhole cover.

structures, such as curves, regions, and junctions, are efficiently detected, even with the existence of high-level noise.

Within the voting field, the vote cast by a ball tensor is achieved by summing the votes cast by stick tensors that span 360° at regular intervals (Zou et al. 2012). The vote cast by a stick tensor is defined by a decay function, D (Mordohai and Medioni 2006) in Equation (1):

$$D(s,\kappa,\sigma) = \exp\left(-\frac{s^2 + c\kappa^2}{\sigma^2}\right) \tag{1}$$

where s denotes the arc length between the voter and the receiver, σ is the voting scale, κ is the curvature, and c controls the degree of decay defined by Equation (2) (Mordohai and Medioni 2006):

$$c = \frac{-16\log_2(0.1) \times (\sigma - 1)}{\pi^2} \tag{2}$$

To efficiently extract pavement marking pixels from the thresholded image, we develop a multi-scale tensor voting framework that utilizes ball tensors to infer region elements. At the beginning of the iterative multi-scale ball voting procedure, a large voting scale, σ, is selected to efficiently suppress noise. During the following iterations, to focus more on preserving local details, the voting scale is repetitively decreased by an interval, $\Delta\sigma$. To realize the smallest voting field where tensors can cast votes, the iterative multi-scale ball voting procedure ceases when the voting scale reaches a stop criterion, σ_e. After the iterative multi-scale ball voting, a general second-order, symmetric, non-negative definite tensor is generated at each location of the manhole cover candidates. These tensors are represented by covariance matrices as follows (Mordohai and Medioni 2006):

$$\mathbf{T} = (\lambda_1 - \lambda_2)\boldsymbol{e}_1\boldsymbol{e}_1^{\mathrm{T}} + \lambda_2(\boldsymbol{e}_1\boldsymbol{e}_1^{\mathrm{T}} + \boldsymbol{e}_2\,\boldsymbol{e}_2^{\mathrm{T}}) \tag{3}$$

where λ_1 and λ_2 ($\lambda_1 \geq \lambda_2$) are the eigenvalues of matrix $\mathbf{T}$; $\boldsymbol{e}_1$ and $\boldsymbol{e}_2$ are the corresponding eigenvectors in Equation (3). In the standard tensor voting framework, λ_2 reflects well the saliency of a region structure (Mordohai and Medioni 2006). Therefore, with the values of λ_2 from all tensors, we generate a saliency map, in which the saliency of a pixel indicates the probability of that pixel being located within a region. Figure 2(*c*) shows a generated saliency map via the proposed multi-scale tensor voting.

2.3. Extraction

Afterwards, manhole covers are extracted by successively applying Euclidean distance clustering and morphological operations. Through multi-scale tensor voting, manhole covers are mostly extracted. However, as shown in Figure 2(*d*), some small fragments are falsely detected as manhole covers. To further remove those small fragments that are not likely to be manhole covers, a Euclidean distance clustering approach is proposed. The extracted manhole cover pixels are grouped into clusters based on the Euclidean distances to their neighbours with a clustering distance of d_c pixels. Specifically, an unclustered manhole cover pixel is grouped into a specific cluster, if and only if, its shortest Euclidean distance to the elements within this cluster lies below d_c. After all manhole cover pixels are labelled with a specific cluster, a bounding rectangle is calculated for each

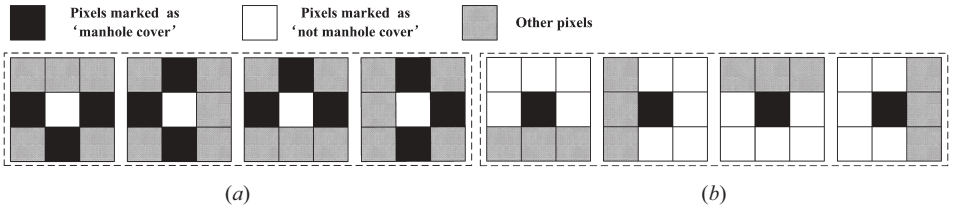

Figure 3. Structural templates for (*a*) hole filling and (*b*) boundary smoothing.

cluster. Then, the clusters, whose diagonals of the bounding rectangles are smaller than a pre-defined refinement threshold, $d_{\min}$, are regarded as not being manhole covers and filtered out.

To obtain accurate manhole covers, a template-driven refinement operation is used for refining the extracted results. The refinement techniques probe manhole covers with a pre-defined small shape or template called a structuring element; the structuring element in this article is defined in Figure 3.

These structuring elements are used as sliding windows to examine the pixels located at the centre of a sliding window. As shown in Figure 3(*a*), we define four structural templates to examine non-manhole cover pixels for filling in holes. Similarly, as shown in Figure 3(*b*), we define four structural templates to smooth the boundary pixels of a manhole cover. The refinement commences with an iterative hole filling process, which iteratively applies hole filling structural templates to the extracted manhole covers. During each iteration, the holes inside manhole covers are gradually filled in. This process ceases when no further holes need to be filled in. Subsequently, an iterative edge smoothing process is carried out to iteratively smooth irregular manhole cover boundaries. As shown in Figure 2(*e*), after a successive combination of hole filling and edge smoothing, the extracted manhole covers are efficiently refined.

3. Results and discussion

A set of experiments were carried out to evaluate the stability and capability of the proposed manhole cover extraction using GRF images. To objectively evaluate the performance, we used the manual interpretations of the manhole covers in these GRF images as the ground truth.

3.1. Data sets

A group of GRF images was generated from the mobile LiDAR point clouds acquired on April 23, 2012, by a RIEGL VMX-450 system in Xiamen, a port city with a subtropical urban environment, in southeast China. The minivan travelled at approximately 50 km/hour along Huandao Road, a typical urban road area with high buildings, dense vegetation, and traffic signposts on both sides. At a vehicle speed of 50 km/hour, the average point density was estimated as 286.44 points/m^2 with a scan rate of 200 lines/s. Particularly, the point density for the Huandao road surface is as high as 4000–7000 points/m^2. A 3-km road section containing 231.7 million points was selected. The road surface points were first extracted from the selected dataset in the pre-processing stage. According to the high point density of the surveyed road, the grid cell, S_p, was set to 3 cm for generating a GRF image from the segmented road points.

3.2. Extraction of manhole covers

To test the performance of our manhole cover extraction strategy, we selected six samples (cases GRF-1–GRF-6) containing manhole covers with different shapes under different conditions, as shown by the GRF images in the first row in Figure 4. To identify manhole cover candidates from the GRF images, the segment width, W_s, was set to 30 pixels, which equals a road width of 1 m. The segmentation threshold was automatically determined by Otsu's method. The identified manhole cover candidates are shown in the second row in Figure 4. Afterwards, in the proposed multi-scale tensor voting method, the voting scales, σ, σ_e, $\Delta\sigma$, were set to 14.0, 5.0, and 4.5, respectively. A saliency map was generated for each sample, as shown in the third row in Figure 4. As seen from the saliency maps, noise shows lower saliencies than those of manhole cover pixels. Therefore, noise is well suppressed, and manhole cover pixels are well preserved. Finally, as shown in the fourth row in Figure 4, manhole covers were extracted by filtering out small fragments, filling in holes, and smoothing boundaries using a cluster distance, d_c, and a refinement threshold, d_{min}, of 2 and 20 pixels, respectively.

Visual inspection shows that, for samples GRF-1, GRF-2, and GRF-3, manhole covers with different shapes (including rectangles and discs) are correctly and completely extracted. For samples GRF-4 and GRF-5, some manhole covers are partially painted with pavement markings; therefore, these manhole covers are incompletely extracted. However, for sample GRF-6, a manhole cover shows higher intensity than its surrounding road surface. Thus, our proposed strategy failed to extract it. Next, by comparing the extraction results with the manually labelled reference data, we performed quantitative evaluations using the following three measures: completeness, correctness, and *F*-measure (Guan et al. 2014). As shown in Table 1, our manhole cover extraction strategy achieves an average completeness of 0.92, an average correctness of 0.89, and an average *F*-measure of 0.90 on the six samples. The proposed strategy shows superior performance on the first three samples. However, because of the existence of pavement markings or

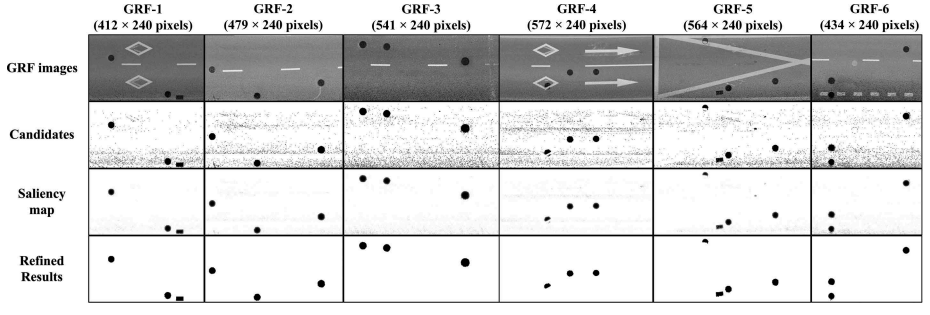

Figure 4. Manhole cover results for small GRF samples (cases GRF-1–GRF-6).

Table 1. Evaluation of results for manhole cover samples (GRF-1–GRF-6).

	GRF-1	GRF-2	GRF-3	GRF-4	GRF-5	GRF-6	Mean
Completeness	1.00	0.99	0.99	0.87	0.87	0.77	0.92
Correctness	0.90	0.87	0.90	0.84	0.87	0.95	0.89
F-measure	0.95	0.93	0.95	0.86	0.87	0.85	0.90

because of the special reflectance of manhole covers, relatively lower performances occur on the last three samples. On the whole, our manhole cover extraction strategy works very well and extracts manhole covers with little loss and incompleteness.

3.3. Comparative study

To further evaluate the performance and feasibility of our manhole cover extraction method, we compared it with the original tensor voting method (Mordohai and Medioni 2006). For this comparative test, we selected three road sections (cases GRF-7–GRF-9). Compared with road sections in samples GRF-1–GRF-6, the roads in samples GRF-7–GRF-9 were newly built, thereby leading to a low intensity contrast with manholes. Figure 5 shows a comparison of the results obtained using both the tensor voting method and our multi-scale tensor voting. Visual inspection indicates that our multi-scale tensor voting method removes noise by iteratively employing a ball voting and a saliency thresholding scheme to delete pixels with low saliency and gradually focusing the votes on only promising regions. As shown in Table 2, our algorithm, achieving an average completeness of 0.86, an average correctness of 0.86, and an average *F*-measure of 0.85, respectively, outperforms the Mordohai's tensor voting in successfully detecting both circular and rectangular manhole covers.

The proposed strategy was implemented using C++ running on an Intel (R) Core (TM) i5-3470 computer with 16.0-GB memory. With only one processing pipeline, the total computing time for processing 3-D points covering a 3-km road surface is approximately 15 minutes. By partitioning the entire road surface into a set of segments with a length of approximately 50 m along the road direction and distributing the set into a multi-thread

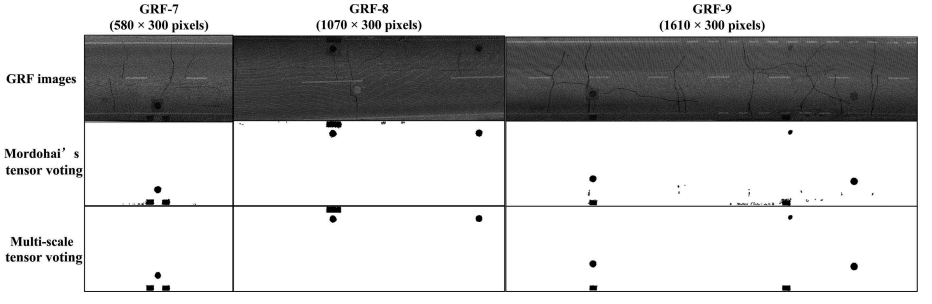

Figure 5. Comparative results of three large manhole cover samples (cases GRF-7–GRF-9).

Table 2. Comparative results for three manhole cover samples (GRF-7–GRF-9).

	Mordohai's tensor voting			Multi-scale tensor voting		
	Completeness	Correctness	*F*-measure	Completeness	Correctness	*F*-measure
GRF-7	0.99	0.79	0.88	0.98	0.93	0.96
GRF-8	0.60	0.75	0.66	0.60	0.86	0.71
GRF-9	0.98	0.57	0.72	0.98	0.80	0.88
Mean	0.86	0.70	0.75	0.86	0.86	0.85

computing environment with four parallel processing pipelines, the computing time is further reduced to 3.8 minutes.

4. Conclusions

In this article, we proposed a novel strategy for rapid inventory mapping of manhole covers from mobile LiDAR data. Our strategy was applied to six manhole cover samples. Through visual inspection and quantitative evaluation, our strategy achieved high degrees of completeness (0.91), correctness (0.87), and *F*-measure (0.89). In addition, over three other manhole cover samples, we compared our multi-scale tensor voting with Mordohai's tensor voting. The comparative study demonstrates that our algorithm achieved the highest correctness and *F*-measure. Although our strategy requires longer computing time to extract manhole covers, multi-thread and parallel computing techniques can be used to further reduce the time complexity and improve the performance of our strategy for the inventory mapping of manhole covers on urban road surfaces.

Acknowledgements

The authors would like to thank Mr M. McAllister for his assistance in proofreading our article and the anonymous reviewers for their constructive comments and suggestions in improving the clarity of the article.

Funding

This work was supported by the Startup Foundation for Introducing Talent of Nanjing University of Information Science & Technology (NUIST) and the National Natural Science Foundation of China [grant 41471379].

References

Broggi, A. 1995. "A Massively Parallel Approach to Real-Time Vision-Based Road Markings Detection." In *Proceedings of the Intelligent Vehicles '95 Symposium*, Detroit, MI, September 25–26, 84–89. Piscataway, NJ: IEEE Computer Society. doi:10.1109/IVS.1995.528262.

Cheng, H., N. Zheng, X. Zhang, J. Qin, and H. Van De Wetering. 2007. "Interactive Road Situation Analysis for Driver Assistance and Safety Warning Systems: Framework and Algorithms." *IEEE Transactions on Intelligent Transportation Systems* 8 (1): 157–167. doi:10.1109/TITS.2006.890073.

Golparvar-Fard, M., V. Balali, and J. de la Garza. 2012. "Segmentation and Recognition of Highway Assets Using Image-Based 3D Point Clouds and Semantic Texton Forests." *Journal of Computing Civil Engineering* 1943-5487, 1–14. doi:10.1061/(ASCE)CP.1943-5487.0000283.

Guan, H., J. Li, Y. Yu, C. Wang, M. Chapman, and B. Yang. 2014. "Using Mobile Laser Scanning Data for Automated Extraction of Road Markings." *ISPRS Journal of Photogrammetry and Remote Sensing* 87: 93–107. doi:10.1016/j.isprsjprs.2013.11.005.

He, Y., H. Wang, and B. Zhang. 2004. "Color-Based Road Detection in Urban Traffic Scenes." *IEEE Transactions on Intelligent Transportation Systems* 5 (4): 309–318. doi:10.1109/TITS.2004.838221.

Ji, S., Y. Shi, and Z. Shi. 2012. "Manhole Cover Detection Using Vehicle-Based Multi-Sensor Data." In *International Archives of the Photogrammetry, Remote Sensing and Spatial Information Sciences*, Vol XXXIX-B3, 2012 XXII ISPRS Congress, edited by M. Shortis, N. Paparoditis, and C. Mallet, Melbourne, August 25–September 1, 281–284. doi:10.5194/isprsarchives-XXXIX-B3-281-2012.

McCall, J., and M. Trivedi. 2006. "Video-Based Lane Estimation and Tracking for Driver Assistance: Survey, System, and Evaluation." *IEEE Transactions on Intelligent Transportation Systems* 7 (1): 20–37. doi:10.1109/TITS.2006.869595.

Mordohai, P., and G. Medioni. 2006. *Tensor Voting: A Perceptual Organization Approach to Computer Vision and Machine Learning*. San Rafael, CA: Morgan & Claypool Publishers. doi:10.2200/S00049ED1V01Y200609IVM008.

Olsen, M., G. Roe, C. Glennie, F. Persi, M. Reedy, D. Hurwitz, K. Williams, H. Tuss, A. Squellati, and M. Knodler. 2013. "National Cooperative Highway Research Program (Report 748): Guidelines for the Use of Mobile LIDAR in Transportation Applications." Washington, DC: Transportation Research Board. http://www.national-academies.org/trb/bookstore

Otsu, N. 1979. "A Threshold Selection Method from Gray-Level Histograms." *IEEE Transactions on Systems, Man, and Cybernetics* 9 (1): 62–66. doi:10.1109/TSMC.1979.4310076.

Pikus, I. M. 2006. "Manhole Security: Protecting America's Critical Underground Infrastructure." White Paper, 2006. Washington, DC: National Strategies.

Tanaka, N., and M. Mouri. 2000. "A Detection Method of Cracks and Structural Objects of the Road Surface Image." In *IAPR Workshop on Machine Vision Applications* (MVA2000), Tokyo, November 28–30, 2000, 387–390.

Timofte, R., and L. Gool. 2011. "Multi-View Manhole Detection, Recognition, and 3D Localization." In *2011 IEEE International Conference on Computer Vision Workshops* (ICCV Workshops), Barcelona, November 6–13, 2011, 188–195. doi:10.1109/ICCVW.2011.6130242.

Williams, K., M. Olsen, G. Roe, and C. Glennie. 2013. "Synthesis of Transportation Applications of Mobile LIDAR." *Remote Sensing* 5 (9): 4652–4692. doi:10.3390/rs5094652.

Xue, J., and D. Titterington. 2011. "T-Tests, F-Tests and Otsu's Methods for Image Thresholding." *IEEE Transactions on Image Processing* 20 (8): 2392–2396. doi:10.1109/TIP.2011.2114358.

Zou, Q., Y. Cao, Q. Li, Q. Mao, and S. Wang. 2012. 'Cracktree: Automatic Crack Detection from Pavement Images.' *Pattern Recognition Letters* 33 (3): 227–238. doi:10.1016/j.patrec.2011.11.004.